Journal of Control, Automation and Electrical Systems
https://doi.org/10.1007/s40313-025-01173-6

Master-Slave Synchronization for Parameter Estimation of Photovoltaic Module Model

Gustavo Henrique de Paula Santos[1] · Bader Sager[2] · Fekadu Shewarega[2] · Hendrik Vennegeerts[2] · Moisés Carlos Tanca Villanueva[3] · Elmer Pablo Tito Cari[1]

Received: 3 May 2024 / Revised: 24 January 2025 / Accepted: 24 April 2025

Abstract

Photovoltaic systems are the most mature and promising technology for the generation of clean electricity. However, due to their non-convex, nonlinear, and multi-parametric characteristics, models and methods must be developed for optimizing their operation in different environments and conditions for forecasting power and determining the efficiency of a PV plant. Several algorithms have aimed at accurately defining the parameters and most of them focus on improving both exploration and exploitation of the method by combining different techniques. On the other hand, a simple change in a model can improve the accuracy of parameters. This study proposes a small alternation in the model, i.e., inclusion of synchronization inputs by master-slave coupling between real and mathematical systems. The coupling was used with swarm mean-variance mapping optimization (Swarm MVMO) metaheuristic method and applied to a photovoltaic module model (PVM) for different temperature and irradiance measurements. The results showed an improvement in the estimated parameters after the aforementioned inclusion in comparison with another method from the literature.

Keywords Swarm MVMO · Photovoltaic model · Photovoltaic system · Parameter estimation · Metaheuristic method · Master-slave coupling

1 Introduction

Photovoltaic (PV) systems are the most mature and promising technology for electric power generation in the clean energy portfolio (Gao et al. 2021) and have excelled in the world energy matrix (Lopes et al. 2021). In Brazil, the PV installed power, with 39.8 GW (17%), has become the second source of energy in the electrical energy matrix and is expected to become the first in 2040 (ABSOLAR 2024). Toward supporting its management, numerical methods have been adopted for predicting photovoltaic power, which depends on the accuracy of the model parameters, of which the correct ones can enhance efficiency in a new project or accurately depict the system's operation in a real-world scenario. That is crucial, since the characteristics of PV cells can change over time due to factors such as aging, degradation, failures, maintenance, dirt, soil, and weeds (Hara et al. 2022).

Bader Sager, Fekadu Shewarega, Hendrik Vennegeerts, Moisés Carlos Tanca Villanueva, and Elmer Pablo Tito Cari. These authors contributed equally to this work.

✉ Gustavo Henrique de Paula Santos
gustavohenriquesantos@usp.br

Bader Sager
bader.sager@uni-due.de

Fekadu Shewarega
fekadu.shewarega@uni-due.de

Hendrik Vennegeerts
hendrik.vennegeerts@uni-due.de

Moisés Carlos Tanca Villanueva
mtanca@unsa.edu.pe

Elmer Pablo Tito Cari
elmerpab@sc.usp.br

[1] Department of Electrical Engineering and Computing, University of São Paulo, São Carlos, São Paulo, Brazil

[2] Institute of Electrical Energy Systems, University of Duisburg-Essen, Duisburg, North Rhine-Westphalia, Germany

[3] Department of Electrical Engineering, National University of San Agustin de Arequipa, Arequipa, Arequipa, Peru

Published online: 31 May 2025

The main approaches for parameter estimation of PV models are analytic, numeric, and metaheuristic methods (Huynh et al. 2022), of which the former represents the PV model by mathematical equations for finding the unknown parameters using datasheet information (Xu 2022). The analytic method generalizes all *I-V* curve measurement data using selected points. If a point assignment is incorrect, the error of the estimated parameter can be significant (Long et al. 2020). Simplicity, computational efficiency, and easy implementation are its advantages, since only one iteration is required for the obtaining of a desired result (Tchakpedeou et al. 2022).

Numerical methods usually adopt nonlinear programming algorithms to identify unknown parameters (Diab et al. 2020). The estimated parameters are obtained by *I-V* and *P-V* curve fitting through error minimization between measured and estimated data (Jiao et al. 2020). The accumulation of errors between the points decreases the precision of the parameters, and drawbacks associated with those methods include considerable computational efforts, difficult selection of appropriate initial parameters for the algorithm, and their vulnerability to local optima (Ridha et al. 2022; Kumar and Magdalin Mary 2022). Some numerical methods applied to PV models can be found in Ćalasan et al. (2021) and Sharadga et al. (2021).

Metaheuristic methods are some of the most efficient techniques for estimating the parameters of PV systems (Abdel-Basset et al. 2022). The estimation of unknown parameters is based on global optimization algorithms, which offer robust solutions to complex problems and achieve satisfactory results in comparison with analytical and numerical methods. Their main advantages are no restriction on the objective function continuity and simple implementation (Xiong et al. 2021; Luo and Yu 2022; Paul et al. 2022).

Most research on the estimation of parameters of photovoltaic systems focuses on the combination of different metaheuristic algorithms toward improving both exploration and exploitation of the method. Ramadan et al. (2022) combined a hunter-prey and wild horse optimizer for estimating the three-diode model (TDM) parameter based on root-mean-square error (RMSE) and Abdel-Basset et al. (2022) mixed generalized normal distribution, marine predator, and whale optimizer for estimating the parameter of single-diode model (SDM) and double-diode model (DDM). Batzelis et al. (2022) proposed using the Euclidean distance metric instead of a current distance one in the objective function. The approach seems useful especially when the measurement is noisy, although a small improvement in RMSE is achieved. The aforementioned studies aimed at improvements in the algorithm, disregarding modifications to the model. However, an improvement in parameter estimation can be achieved through small changes to the model equation. Xu (2022) proposed a simplification of the model, transforming the nonlinear problem into a linear one. Although small improvements were achieved in relation to RMSE, the computational burden decreased, which would be useful for online applications. Huang et al. (2020) designed an approach that included a pre-treatment of model parameters prior to estimation. Based on a sensitivity analysis, an index first identifies parameters of greatest influence on the model output, which are then estimated by HCSS algorithm. The advantage of the approach is the possibility of evaluating the model parameters prior to estimation. New research included the parameter for photovoltaic systems under shading conditions (Ma et al. 2022) and for bifacial modules (Ahmed et al. 2023). Ma et al. (2022) divided SDM into two stages for including a bypass diode and Ahmed et al. (2023) included an extra parameter (additional series resistance) in the model toward considering the extra power gain for the bifacial module.

This paper proposes a new small change to the PVM model by including a master-slave coupling (Cari et al. 2009) toward improving the accuracy of the estimated parameters. Swarm MVMO, a metaheuristic method, estimated the parameters, and a sensitivity analysis (SA) selected the best synchronization input in the model.

1.1 Contributions

The main contributions of this research are *i*) proposal of a master-slave coupling in PVM for improving the accuracy of estimated parameters, *ii*) development of a new Swarm MVMO for exploration and exploitation searches of photovoltaic system parameters, and *iii*) a comparative analysis of the results with those from previous research and swarm MVMO with and without synchronization coupling.

2 Photovoltaic module model

The models mostly adopted for representing PV systems are SDM, DDM, TDM, and PVM. The first three employ a single PV cell and the fourth uses a complete PV module (Abdel-Basset et al. 2022; Gao et al. 2021; Ramadan et al. 2022). SDM is the most adopted one due to its simplicity, precision, and fewer computational efforts (Huynh et al. 2022; Yu et al. 2022b). In a cell represented by SDM (Fig. 1a), its photogenerated current (I_{ph}) expresses the irradiance level at the cell (Ma et al. 2022) and I_d denotes the diffusion current at the P-N junction of the diode. The series resistance (R_s) accounts for the contact resistance among silicon and electrode surfaces, electrode resistance, and current flow resistance, shunt resistance (R_{sh}) represents the leakage current of a P-N junction diode by the shunt current (I_{sh}) (Ramadan et al. 2022; Eslami et al. 2022), and I_c and V_c are the cell output current and voltage, respectively.

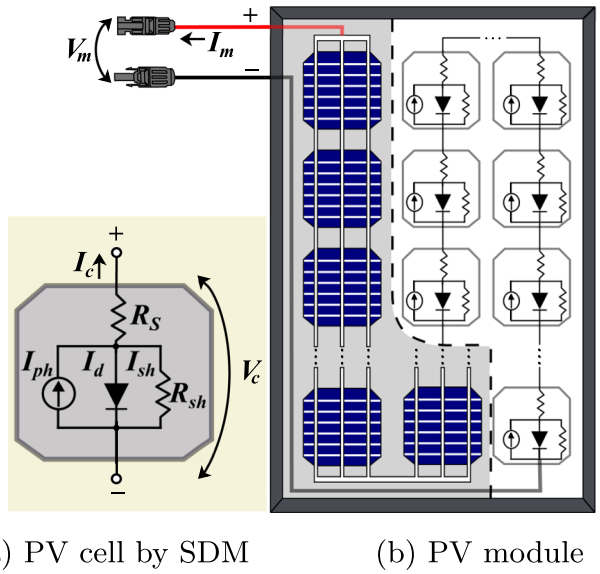

Fig. 1 PV power generation units: 1a) cell and 1b) module, both based on SDM (Adapted from Tong and Pora (2016) and El-Naggar et al. (2012))

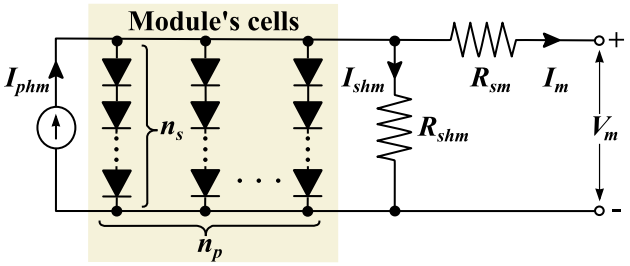

Fig. 2 PV module model (PVM) electrical circuit (Adapted from Nguyen et al. (2022))

This section focuses on the electrical circuit and mathematical equations of PVM addressed in the next section for parameter estimation. SDM, DDM, and TDM equations are not provided due to space limitations. However, the procedure reported in the next section can be applied for those models only by changing the proper input, output, and parameter vector. A PV module (Fig. 1b) is typically composed of interconnected cells, where I_m and V_m denote module output current and voltage, respectively. Once such cells are represented by SDM and assuming all cells are identical and receive the same irradiance level for producing the same current and voltage, PVM shows, in a single circuit, the combined effects resulting from the cells' connection (Fig. 2), where n_s and n_p are number of cells in series and parallel connection, respectively.

The circuit in Fig. 2 is modeled in:

$$I_{phm} - I_{sm}\left\{\exp\left[\frac{q(V_m + R_{sm} I_m)}{a_m k T_m}\right] - 1\right\} - \frac{V_m + R_{sm} I_m}{R_{shm}} - I_m = 0 \tag{1}$$

where I_{phm} is the module photo-generated current, I_{sm} is the module diode reverse saturation current, R_{sm} and R_{shm} are module series and shunt resistances, respectively, a_m is the module equivalent diode ideality factor, T_m is the module temperature (K), q is the electron charge ($1.60217646 \times 10^{-19}$ C), and k is Boltzmann constant ($1.3806503 \times 10^{-23}$ J/K). PVM has five unknown parameters, namely I_{phm}, I_{sm}, R_{sm}, R_{shm}, and a_m. Equation (1) can be modeled by a system according to:

$$0 = f(u, y, p) \tag{2}$$

where $u = [V_m]$ is the input vector, $y = [I_m]$ is the output vector, and $p = [I_{phm}, I_{sm}, a_m, R_{sm}, R_{shm}]$ is the parameter vector.

3 Master-slave synchronization for parameter estimation

The parameter estimation problem is formulated as an optimization problem in which a parameter fitting algorithm minimizes fitness function (objective function) $J(p)$, as described in:

$$J(p) = \sqrt{\frac{1}{N}\sum_{j=1}^{N}(y_r - y(p))^2} \tag{3}$$

where N is the sampling number and y_r and y are the outputs of real system and mathematical model, respectively. A simple incorporation of some output of the real system in the mathematical model (u_{syn}) enhances the estimation process. Such a type of coupling is known as master-slave synchronization and has been used in communication systems (Gameiro and Rodrigues 2001) (see Fig. 3) and for estimating parameters of chaotic systems (Cari et al. 2009).

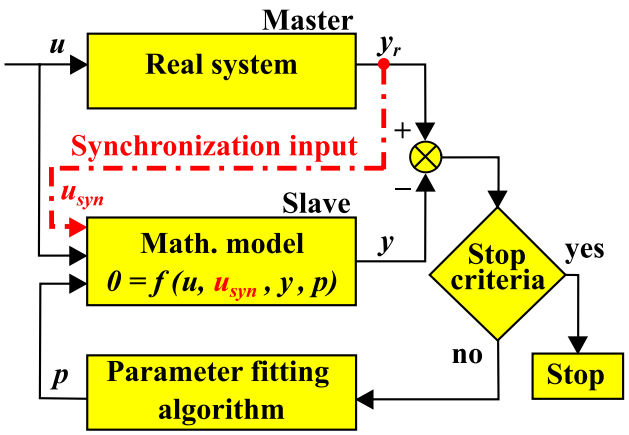

Fig. 3 Master-slave synchronization

After the inclusion of synchronization inputs, the parameter estimation problem can be seen as a synchronization one, in which the slave system output synchronizes with the master system after the application of the parameter fitting algorithm. More information about master-slave synchronization can be found in Gameiro and Rodrigues (2001).

4 Swarm Mean-Variance Mapping Optimization

Mean-variance mapping optimization (MVMO) is a metaheuristic algorithm that uses concepts of evolutionary algorithms, such as selection, mutation, and crossover applied to a strategic transformation of mutated genes from offspring based on mean-variance of the n-best population. It expands the original MVMO using swarm-based methods and a multi-parent crossover strategy toward enhancing search diversity while maintaining a trade-off between exploration and exploitation (Rueda et al. 2015). Figure 4 displays detailed concepts of Swarm MVMO, where i is the function evaluation counter, c is the particle counter, m is the number of particles, i_{max} is the maximum number of fitness function evaluations, and *rand* is a random uniform number between [0, 1].

4.1 Setup

The setup stage initializes with the definitions of m, number of parameters to be estimated (p_n) and that constitute an individual, number of individuals in each particle (X_n), and range of lower (p_{min}) and upper (p_{max}) bounds of each parameter. Individuals are randomly generated between limits p_{min} and p_{max} for each parameter. The values are then normalized in space [0, 1] for guaranteeing the offspring generation stage never violates the limits. The values of i_{max} and m are determined by:

$$i_{max} = 10000.p_n \tag{4}$$

$$m = 15.p_n \tag{5}$$

where factors 10000 and 15 are based on statistical tests, evaluation of convergence performance, and the final solution quality, according to recommendations of Rueda and Erlich (2013).

4.2 Fitness evaluation

At this stage, all parameter values of each individual and particle are de-normalized from [0, 1] to their original values. The procedure begins with the loading of measured data from the PV module for which the parameters will be estimated and calculates the output current for each individual

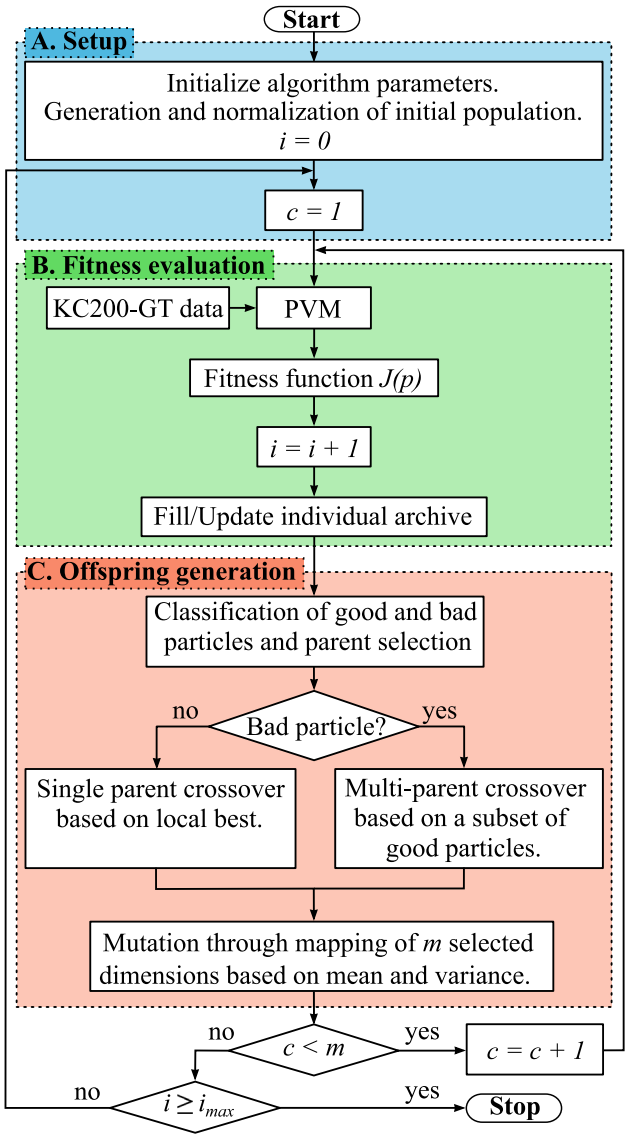

Fig. 4 Swarm MVMO algorithm (Adapted from Sager and Erlich (2017))

in all particles according to the model in (1) and the objective function in (3).

The solution archive works as adaptive memory and stores the n-best results based on the fitness function, ranked in an ascending order from lowest to highest. The global best is the individual with the best value of all particles and the local best is the best in a particle. The archive is updated only when a better fitness value has been identified, and both mean and variance for optimization variables are computed and stored. The recalculation of mean and variance values is required when a solution has been removed. Such factors are used as inputs for the mapping function to generate new offspring. Figure 5 illustrates the solution archive for the PVM model which has five unknown parameters ($p_n = 5$), where X is one of the individuals of the particle and p_i is one of the parameters of the individual.

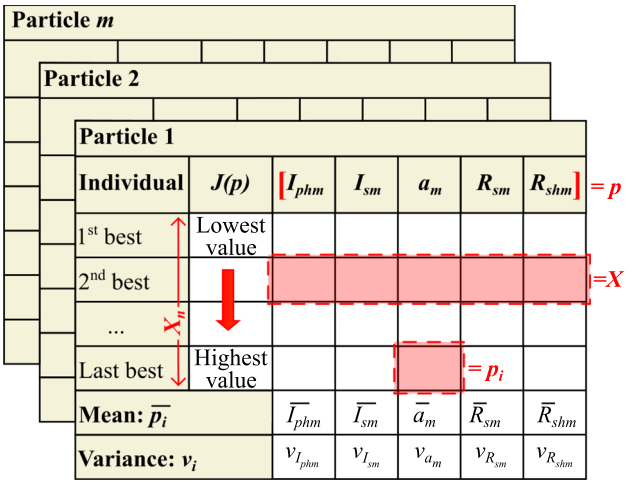

Fig. 5 Swarm MVMO solution archive for PVM (Adapted from Rueda and Erlich (2013))

4.3 Offspring generation

As shown in Fig. 6, the offspring generation stage begins with the categorization of all particles. Each particle is represented by its respective individual with the smallest value of the objective function (local best). Subsequently, the particles are ranked according to their local best values and two distinct groups, namely good group (GG) and bad group (BG), are formed. GG comprises 20% of the top-performing particles, determined by their optimal local best values, whereas BG consists of 70% of the lowest-performing particles, based on their local best (worst values). Additionally, 10% of the particles located between GG and BG remain unchanged for ensuring diversity. The percentage value for the separation of particles into GG and BG was based on experiences and is recommended for most applications. In GG, the parent for the next generation (X_G^{parent}) is the global best individual (X_i), as described in:

$$X_G^{parent} = X_i \tag{6}$$

whereas for BG, the parent (X_B^{parent}) is selected by a multi-parent strategy aimed at enhancing performance by balancing exploration and exploitation according to:

$$X_B^{parent} = X_c + \beta(X_i - X_j) \tag{7}$$

where X^{parent} is the parent for GG or BG, respectively, in generation n, X_i is the global best particle in GG, X_j is the last good particle in GG, X_c is a random intermediate particle between X_i and X_j in GG, and β is a random number for re-drawing any element outside the [0, 1] range.

Some genes contained in vector X^{parent} are randomly selected by mutation in the mutation process. A new individual child X^{new} is generated from X_G^{parent} and X_B^{parent}

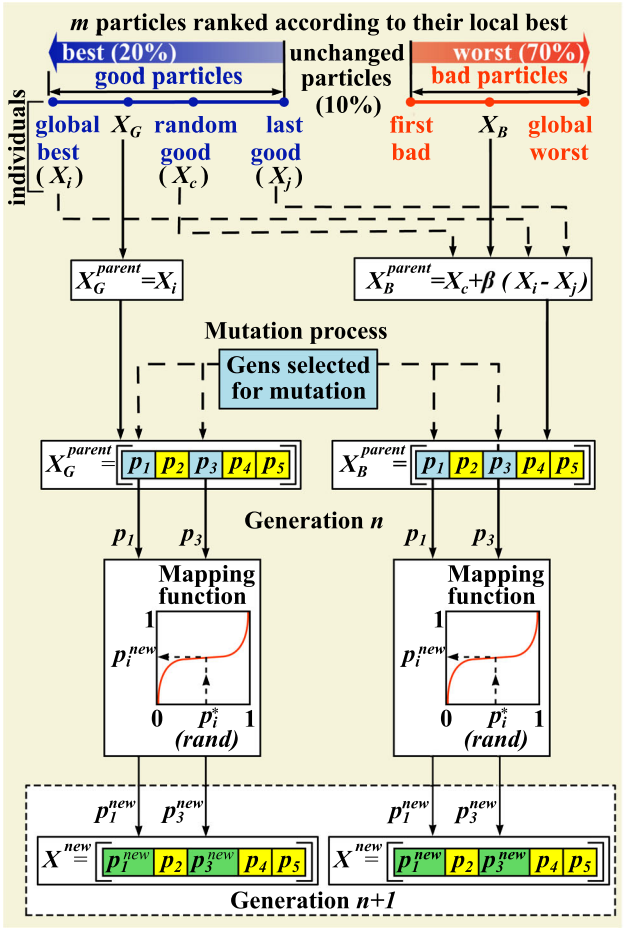

Fig. 6 Detailed scheme of offspring generation (Adapted from Rueda and Erlich (2013))

through an alteration in the genes selected for mutation by the mapping function, described for the $n+1$ generation in:

$$p_i^{new} = h_p + (1 - h_1 + h_0)p_i^* - h_0 \tag{8}$$

$$h_p = h(p_i = p_i^*)$$

$$h_0 = h(p_i = 0)$$

$$h_1 = h(p_i = 1) \tag{9}$$

$$h(\bar{p}_i, s_1, s_2, p_i) = \bar{p}_i(1 - e^{-p_i s_1}) + (1 - \bar{p}_i)e^{-(1-p_i)s_2} \tag{10}$$

$$s_{1\ or\ 2} = -ln(v_i)\, f_s \tag{11}$$

where h_p, h_1, and h_0 are the outputs of the mapping function, $\bar{p}_i$ is the mean of a parameter, p_i^* is a random number between [0, 1], and $s_{1\ or\ 2}$ is the shape factor based on variance v_i of a parameter and scaling factor f_s, which enables an automatic adjustment of $s_{1\ or\ 2}$ throughout the iterations.

The newly generated individual (X^{new}) is incorporated into its corresponding particle, such that each particle com-

prises $X_n + 1$ individuals (non-applicable to particles that remain unchanged). Subsequently, all $X_n + 1$ individuals of each particle undergo a fitness evaluation and are re-ranked. The least fit individual is then removed. At this moment, the number of individuals in each particle returns to its original value (X_n) and the process starts again in a new iteration. The mapping function is the core of MVMO and uses statistical attributes of the search dynamics by mutation operation based on the mean and variance of the n-best solutions attained, which are saved in a continually updated archive. Figure 6 shows the scheme of good and bad group sizes and the process for the next parent generation, random selection for mutation, and mutation by the mapping function. The PV parameter estimation process by swarm MVMO ends when the maximum number of function evaluations has been reached. More information on MVMO can be found in Rueda and Erlich (2013).

5 Results and discussion

5.1 Measurement data and setup

For comparison purposes, datasets from KC200-GT module, which has 54 multi-crystalline cells and 200 W of power, were used. The data obtained in Huynh et al. (2022); Nguyen et al. (2022); Yu et al. (2022a, b) are composed of real voltage and current ($V_{m,r}$ and $I_{m,r}$) at the output of the module. Such measurement data are widely used and replicate conditions akin to real-world operational scenarios that account for fluctuations in temperature and irradiance levels throughout the day. This study encompassed seven distinct cases, as shown in Table 1. The settings of swarm MVMO algorithm are provided in Tables 2 and 3, which show the parameter search region adopted in this research and in Nguyen et al. (2022), Yu et al. (2022b), and Yu et al. (2022a).

MATLAB R2022b and 8th Gen Intel®Core™ i7-8565U @ 1.80 GHz 1.99 GHz, 16 GB RAM laptop were used for the simulations. Swarm MVMO was run 30 times for all cases. Table 6 of Appendix details the real measured data ($V_{m,r}$ and $I_{m,r}$) in columns 2 and 3 and the estimated magnitudes of current (I_m) and power (P_m) in columns 4 and 7 obtained by swarm MVMO for all cases.

Table 1 Study cases—KC200-GT dataset

Cases	1	2	3	4	5[1]	6	7
T_m (° C)	25	25	25	25	25	50	75
G (W/m^2)	200	400	600	800	1000	1000	1000

[1] Standard test conditions (STC)

Table 2 Setup of Swarm MVMO

Description	Value
Number of parameters to be estimated (p_n)	5
Number of individuals per particle (X_n)	5[1]
Max. number of fitness evaluation (i_{max}), (4)	50000[1]
Number of particles (m), (5)	75[1]

[1]Rueda and Erlich (2013)

Table 3 Parameter search regions

Search region		I_{phm} (A)	I_{sm} (μA)	R_{sm} (Ω)	R_{shm} (Ω)	a_m (-)
In this study	p_{min}	0	0	0.01	100	54
	p_{max}	10	50	0.5	1000	108
Ref.[1]	p_{min}	0	0	0.01	100	1
	p_{max}	10	50	0.5	1000	60
Ref.[2]	p_{min}	0	0	0	0	1
	p_{max}	$0.2 \times I_{sc}$[3]	50	2	5000	4

[1] Nguyen et al. (2022)
[2] Yu et al. (2022b) and Yu et al. (2022a)
[3] I_{sc} is the short-circuit current from the manufacturer's datasheet with value of 8.21 A

Table 4 Parameters ranked according to their influence on the output for case 5

	Higher		⟷		Lower
$\|\|\partial y/\partial p_i\|\|$	3.69E + 9	11.55	3.42	1.98	0.0017
p_i	I_{sm}	R_{sm}	I_{phm}	a_m	R_{shm}

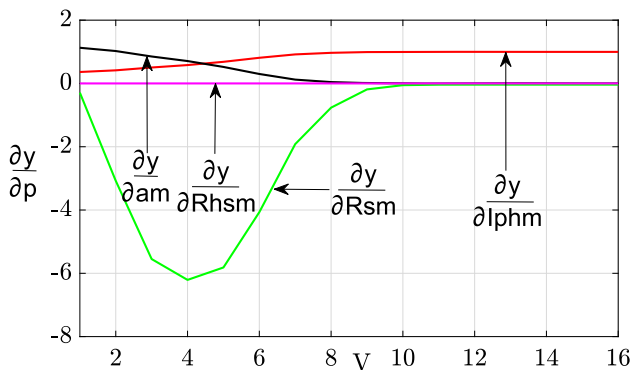

Fig. 7 Sensitivity function of y regarding I_{phm}, R_{sm}, R_{shm}, and a_m

5.2 Sensitivity analysis of PVM

Prior to the estimation of the model parameters, a sensitivity analysis quantified the influence of each parameter on the output. Partial derivatives $\partial y/\partial p_i$ of case 5 (STC) were calculated for such a purpose (see Figs. 7 and 8).

The parameters were ranked according to their influence on the model output by calculating $||\partial y/\partial p_i||$ (Table 4),

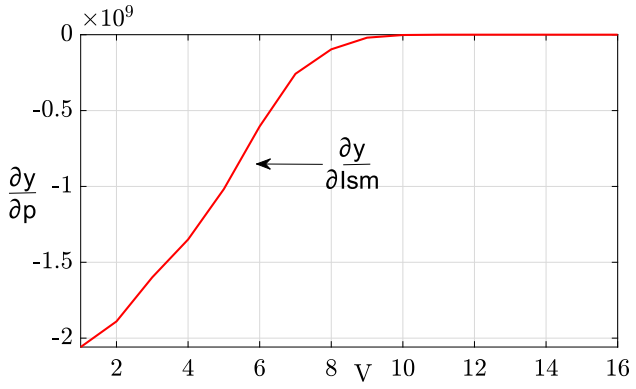

Fig. 8 Sensitivity function of y regarding I_{sm}

where R_{shm} shows an extremely low influence and, therefore, must be the harder parameter to be estimated.

The recognition of the parameters ranked according to their influence on the output serves for the selection of the master-slave coupling in the next stage.

5.3 Swarm MVMO and master-slave synchronization

Figure 9 shows the application of swarm MVMO with master-slave synchronization. The output of master system ($I_{m,r}$) was used as a synchronization output of slave system ($u_{syn} = [I_{m,r}]$) and replaced some variables in PV model. The best result was obtained by substituting $I_{m,r}$ in part of the equation associated with parameter R_{shm}, which agrees with the sensitivity analysis shown in Table 4, since R_{shm} is the most difficult parameter to be estimated. The choice of best place for the replacement of master-slave coupling is still open research. More information can be found in Gameiro and Rodrigues (2001).

5.4 Comparison of the results according to the minimum RMSE

Swarm MVMO estimated the parameter of the model (1) with the algorithm setup of Section 5.1. Table 5 shows the results without (MVMO) and with master-slave synchronization (MVMO$_{syn}$) including those of Nguyen et al. (2022) with artificial ecosystem-based optimization (AEO) and cuckoo search algorithm (CSA), Yu et al. (2022a) with Laplacian Nelder-Mead Hunger Games Search (LNMHGS), and Yu et al. (2022b) with orthogonal learning gradient-based optimization (OLGBO). The lowest RMSE is highlighted in gray. The numbers expressed with exponent a should be multiplied by 10^{-4} and those with b should be multiplied by 10^{-12}.

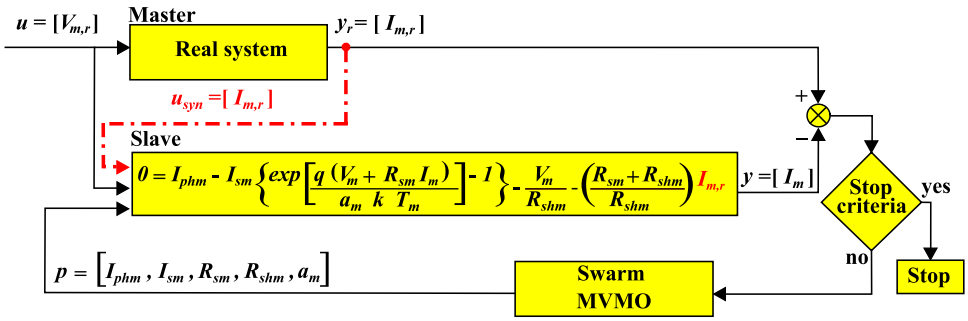

Fig. 9 Swarm MVMO and master-slave looping

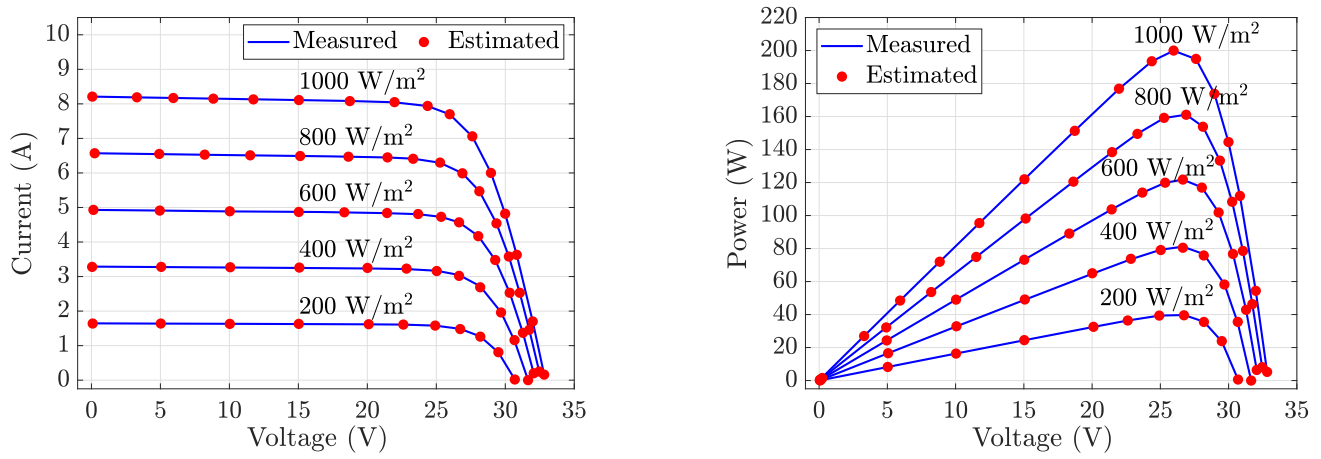

(a) I-V curve (b) P-V curve

Fig. 10 Data measured and estimated by MVMO$_{syn}$—cases 1 to 5: $T_m = 25°\,C$

Table 5 Parameters estimated by swarm MVMO without and with master-slave coupling ($MVMO_{syn}$) and reference values from the literature

Algorithms	I_{phm} (A)	I_{sm} (μA)	R_{sm} (Ω)	R_{shm} (Ω)	a_m (-)	RMSE
Case 1: T_m = 25° C and G = 200 W/m^2						
MVMO	1.6448	0.0004	0.3115	814.00	54.0062	12.56[a]
$MVMO_{syn}$	1.6442	0.0018	0.2189	999.64	58.0377	4.02[b]
AEO	1.6459	0.0002	0.3504	744.27	52.4265	3.57[a]
CSA	1.6469	0.0002	0.3478	745.24	52.6258	8.47[a]
LNMHGS	1.6477	0.0022	1.1275	700.55	1.0000	14.23[a]
OLGBO	1.6460	0.0011	0.4218	708.36	1.0453	14.35[a]
Case 2: T_m = 25° C and G = 400 W/m^2						
MVMO	3.2850	0.0016	0.2882	514.27	57.5265	67.12[a]
$MVMO_{syn}$	3.2833	0.0123	0.2284	819.00	63.5399	2.60[b]
AEO	3.2909	0.0003	0.3393	385.39	53.2043	10.39[a]
CSA	3.2936	0.0002	0.3490	360.83	52.2725	22.86[a]
LNMHGS	3.2898	0.0003	0.6921	723.40	1.0000	13.36[a]
OLGBO	3.2888	0.0006	0.4946	727.82	1.0185	13.50[a]
Case 3: T_m = 25° C and G = 600 W/m^2						
MVMO	4.9284	0.0018	0.2944	321.32	57.7218	81.00[a]
$MVMO_{syn}$	4.9078	0.0213	0.2435	959.46	65.0639	2.19[b]
AEO	4.9354	0.0005	0.3248	263.92	54.3055	34.76[a]
CSA	4.9332	0.0006	0.3202	275.65	54.7780	39.14[a]
LNMHGS	4.9339	0.0055	0.2720	739.38	1.1141	13.49[a]
OLGBO	4.9332	0.0093	0.1763	748.76	1.1296	13.53[a]
Case 4: T_m = 25° C and G = 800 W/m^2						
MVMO	6.5541	0.0052	0.2962	370.33	60.5624	195.86[a]
$MVMO_{syn}$	6.5606	0.0283	0.2644	429.81	65.8660	2.51[b]
AEO	6.5830	0.0002	0.3449	188.37	52.7955	60.01[a]
CSA	6.5672	0.0004	0.3393	228.51	53.7400	81.88[a]
LNMHGS	6.5715	0.0007	0.4593	783.40	1.0415	12.98[a]
OLGBO	6.5695	0.0033	0.2558	806.58	1.0807	13.45[a]
Case 5: T_m = 25° C and G = 1000 W/m^2						
MVMO	8.2113	0.0014	0.3250	207.02	56.9562	134.87[a]
$MVMO_{syn}$	8.1780	0.0422	0.2781	588.57	67.1086	2.16[b]
AEO	8.2296	0.0002	0.3471	149.29	52.4677	11.24[a]
CSA	8.2258	0.0004	0.3394	158.94	53.8729	74.30[a]
LNMHGS	8.2133	0.0008	0.4757	761.91	1.0568	12.06[a]
OLGBO	8.2150	0.0055	0.2854	840.75	1.1116	14.08[a]
Case 6: T_m = 50° C and G = 1000 W/m^2						
MVMO	8.3377	0.0440	0.3243	190.58	61.2457	120.81[a]
$MVMO_{syn}$	8.3147	0.2437	0.3006	507.99	67.2539	0.24[b]
AEO	8.3530	0.0097	0.3469	148.33	52.3781	49.60[a]
CSA	8.3297	0.0182	0.3404	198.02	54.0258	103.70[a]
LNMHGS	8.2970	0.0703	0.3682	826.13	1.0872	14.47[a]
OLGBO	8.2876	0.1407	0.3411	2464.6	1.1258	36.83[a]

Table 5 continued

Algorithms	I_{phm} (A)	I_{sm} (μA)	R_{sm} (Ω)	R_{shm} (Ω)	a_m (-)	RMSE
Case 7: T_m = 75° C and G = 1000 W/m^2						
MVMO	8.4689	0.2982	0.3476	170.34	61.3552	93.27[a]
MVMO$_{syn}$	8.4566	0.5610	0.3371	229.59	63.6824	0.03[b]
AEO	8.4684	0.3348	0.3453	173.12	52.8979	102.70[a]
CSA	8.4546	0.4122	0.3417	210.47	53.5438	112.52[a]
LNMHGS	8.3801	1.2725	0.3503	638.15	1.0846	27.94[a]
OLGBO	8.3803	1.2416	0.3509	625.40	1.0829	28.06[a]

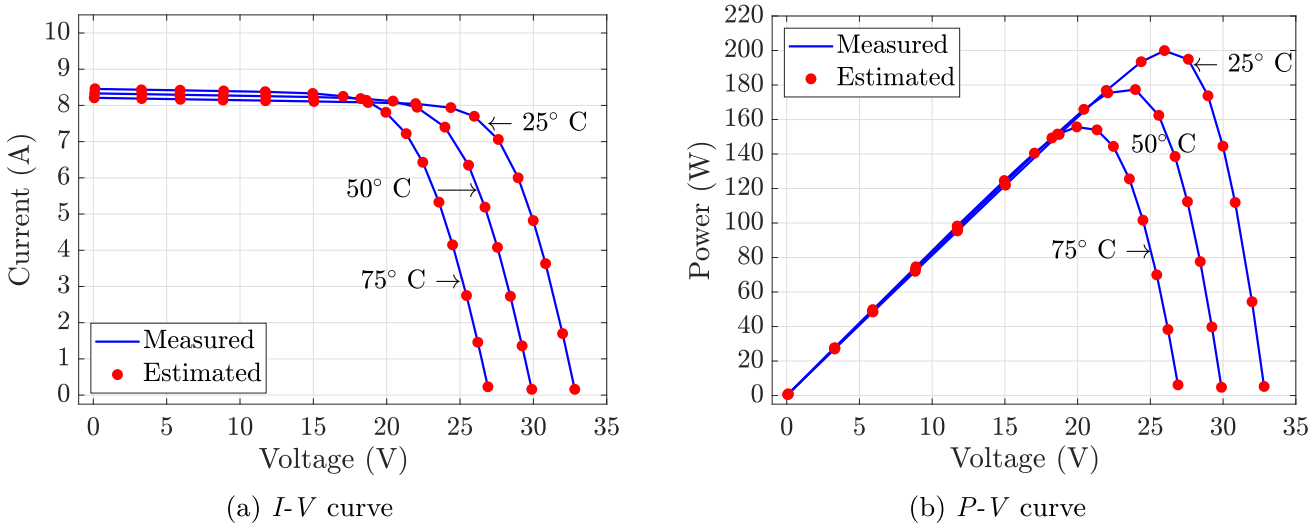

(a) I-V curve (b) P-V curve

Fig. 11 Data measured and estimated by MVMO$_{syn}$—cases 5 to 7: $G = 1000\ W/m^2$

In all tested cases, swarm MVMO with master-slave coupling (MVMO$_{syn}$) showed the lowest RMSE, as expected, since the model seems to be closer to the real system when a synchronization input of master-slave coupling is used. I-V and P-V comparing curves for cases 1 to 5 and 5 to 7 are shown in Figs. 10 and 11, respectively, and the RMSE evolution of MVMO$_{syn}$ in case 5 is displayed in Fig. 12.

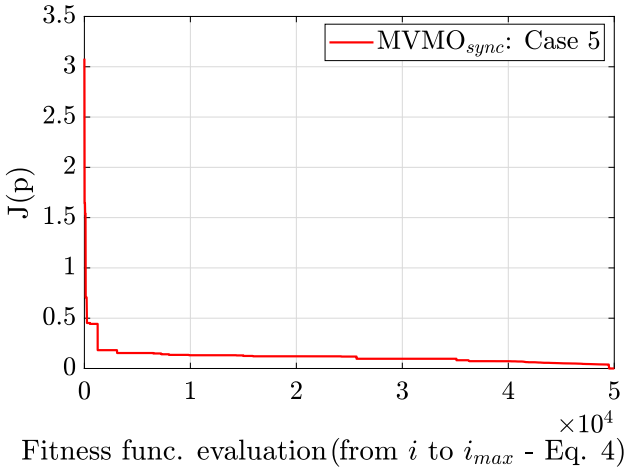

Fig. 12 RMSE evolution of MVMO$_{syn}$ in case 5

6 Conclusions

This paper addressed the introduction of a master-slave coupling in PVM model toward increasing the accuracy of its estimated parameters. The technique is based on the substitution of some outputs of the real system in the mathematical model for approaching both systems. A sensitivity analysis supported the calculation of synchronized inputs and, according to it, R_{shm} was the parameter of least influence on the model output, hence, the most difficult to be accurately estimated. A synchronization input was then proposed in a model term associated with such parameter. Master-slave coupling was used with swarm MVMO for estimating the parameter of PVM from different temperatures and irradiance scenarios and compared with other references. In all the cases, the proposal achieved the lowest RMSE. Although the application of master-slave coupling focused on PVM, it can also be adopted in other PV models. Such topics, including analysis of the best coupling, which is still an open problem, have been addressed in ongoing research.

Acknowledgements The authors acknowledge Duisburg-Essen University / EES Institute for the support during the exchange program that originated this research, Banco Santander, for the academic mobility scholarship PRPG N.º 39/2022, IFSP, for encouraging the first author to attend a doctorate program, and USP, for the opportunities. This research was partially supported by FAPESP, processes 2017/09208-4 and 2017/50389-2 and applied research support process IBA-0043-2017 UNSA.

Appendix Measured and estimated data

Table 6 Comparison between measured and estimated data by Swarm MVMO$_{syn}$ for 7 cases

No	$V_{m,r}$ (V)	$I_{m,r}$ (A)	I_m (A)	$\lvert I_{ae}\rvert$ (A)	$P_{m,r}$ (W)	P_m (W)	$\lvert P_{ae}\rvert$ (W)
Case 1: $T_m = 25°$ C and $G = 200$ W/m^2							
1	30.69	0.02	0.02	0.00	0.61	0.61	0.05
2	29.50	0.80	0.81	0.01	23.60	23.90	0.20
3	28.19	1.27	1.26	0.01	35.80	35.52	0.17
4	26.73	1.49	1.48	0.01	39.83	39.56	0.16
5	24.92	1.58	1.58	0.00	39.37	39.37	0.02
6	22.61	1.61	1.61	0.00	36.40	36.40	0.02
7	20.10	1.62	1.62	0.00	32.56	32.56	0.06
8	15.03	1.63	1.63	0.00	24.50	24.50	0.08
9	10.03	1.63	1.63	0.00	16.35	16.35	0.02
10	5.03	1.64	1.64	0.00	8.25	8.25	0.01
11	0.09	1.65	1.64	0.01	0.15	0.15	0.00
Sum				0.04			0.85
RMSE				0.01			0.15
Case 2: $T_m = 25°$ C and $G = 400$ W/m^2							
1	31.65	0.01	0.00	0.01	0.32	0.00	0.32
2	30.67	1.14	1.16	0.02	34.96	35.58	0.61
3	29.69	1.97	1.96	0.01	58.49	58.19	0.30
4	28.18	2.72	2.69	0.03	76.65	75.80	0.85
5	26.65	3.05	3.02	0.03	81.28	80.48	0.80
6	25.03	3.17	3.16	0.01	79.35	79.09	0.25
7	22.84	3.22	3.23	0.01	73.54	73.77	0.23
8	20.01	3.23	3.25	0.02	64.63	65.03	0.40
9	15.07	3.25	3.26	0.01	48.98	49.13	0.15
10	10.06	3.26	3.27	0.01	32.80	32.90	0.10
11	5.06	3.28	3.28	0.00	16.60	16.58	0.02
12	0.05	3.29	3.28	0.01	0.16	0.16	0.00
Sum				0.17			3.70
RMSE				0.02			0.43
Case 3: $T_m = 25°$ C and $G = 600$ W/m^2							
1	32.06	0.20	0.20	0.00	6.41	6.41	0.00
2	31.28	1.37	1.37	0.00	42.85	42.85	0.00
3	30.32	2.53	2.53	0.00	76.71	76.71	0.00
4	29.27	3.48	3.48	0.00	101.86	101.86	0.00
5	28.04	4.18	4.17	0.01	117.21	116.93	0.28
6	26.65	4.57	4.57	0.00	121.79	121.79	0.00
7	25.35	4.73	4.73	0.00	119.91	119.91	0.00
8	23.68	4.81	4.81	0.00	113.90	113.90	0.00
9	21.43	4.84	4.84	0.00	103.72	103.72	0.00
10	18.33	4.86	4.86	0.00	89.08	89.08	0.00
11	15.03	4.87	4.87	0.00	73.20	73.20	0.00
12	10.03	4.89	4.89	0.00	49.05	49.05	0.00
13	4.95	4.91	4.91	0.00	24.30	24.30	0.00
14	0.14	4.93	4.93	0.00	0.69	0.69	0.00
Sum of absolute error				0.01			0.28
RMSE				0.00			0.07
Case 4: $T_m = 25°$ C and $G = 800$ W/m^2							
1	32.46	0.25	0.25	0.00	8.12	8.12	0.00
2	31.74	1.46	1.46	0.00	46.34	46.34	0.00
3	31.05	2.53	2.53	0.00	78.56	78.56	0.00
4	30.26	3.58	3.58	0.00	108.33	108.33	0.00
5	29.36	4.54	4.54	0.00	133.29	133.29	0.00
6	28.12	5.47	5.47	0.00	153.82	153.82	0.00
7	26.89	5.99	5.99	0.00	161.07	161.07	0.00
8	25.27	6.30	6.30	0.00	159.20	159.20	0.00
9	23.32	6.41	6.41	0.00	149.48	149.48	0.00
10	21.46	6.45	6.45	0.00	138.42	138.42	0.00
11	18.63	6.47	6.47	0.00	120.54	120.54	0.00
12	15.13	6.49	6.49	0.00	98.19	98.19	0.00
13	11.51	6.51	6.51	0.00	74.93	74.93	0.00
14	8.21	6.53	6.53	0.00	53.61	53.61	0.00
15	4.92	6.55	6.55	0.00	32.23	32.23	0.00
16	0.23	6.57	6.57	0.00	1.51	1.51	0.00
Sum of absolute error				0.00			0.00
RMSE				0.00			0.00
Case 5: $T_m = 25°$ C and $G = 1000$ W/m^2							
1	32.82	0.16	0.16	0.00	5.25	5.25	0.00
2	31.99	1.70	1.70	0.00	54.38	54.38	0.00
3	30.83	3.63	3.63	0.00	111.91	111.91	0.00
4	29.99	4.82	4.82	0.00	144.55	144.55	0.00
5	28.96	6.00	6.00	0.00	173.76	173.76	0.00

Table 6 continued

No	$V_{m,r}$ (V)	$I_{m,r}$ (A)	I_m (A)	$\lvert I_{ae}\rvert$ (A)	$P_{m,r}$ (W)	P_m (W)	$\lvert P_{ae}\rvert$ (W)
6	27.61	7.06	7.06	0.00	194.93	194.93	0.00
7	25.97	7.70	7.70	0.00	199.97	199.97	0.00
8	24.37	7.94	7.94	0.00	193.50	193.50	0.00
9	21.97	8.05	8.05	0.00	176.86	176.86	0.00
10	18.73	8.08	8.08	0.00	151.34	151.34	0.00
11	15.04	8.11	8.11	0.00	121.97	121.97	0.00
12	11.74	8.13	8.13	0.00	95.45	95.45	0.00
13	8.84	8.15	8.15	0.00	72.05	72.05	0.00
14	5.93	8.17	8.17	0.00	48.45	48.45	0.00
15	3.30	8.19	8.19	0.00	27.03	27.03	0.00
16	0.06	8.21	8.21	0.00	0.49	0.49	0.00
Sum of absolute error				0.00			0.00
RMSE				0.00			0.00
Case 6: T_m = 50° C and G = 1000 W/m^2							
1	29.89	0.16	0.16	0.00	4.78	4.78	0.00
2	29.23	1.36	1.36	0.00	39.75	39.75	0.00
3	28.43	2.73	2.73	0.00	77.61	77.61	0.00
4	27.55	4.08	4.08	0.00	112.40	112.40	0.00
5	26.70	5.19	5.19	0.00	138.57	138.57	0.00
6	25.58	6.35	6.35	0.00	162.43	162.43	0.00
7	23.97	7.40	7.40	0.00	177.38	177.38	0.00
8	22.07	7.95	7.95	0.00	175.46	175.46	0.00
9	20.43	8.12	8.12	0.00	165.89	165.89	0.00
10	18.23	8.19	8.19	0.00	149.30	149.30	0.00
11	14.99	8.23	8.23	0.00	123.37	123.37	0.00
12	11.76	8.26	8.26	0.00	97.14	97.14	0.00
13	8.86	8.27	8.27	0.00	73.27	73.27	0.00
14	5.89	8.29	8.29	0.00	48.83	48.83	0.00
15	3.32	8.31	8.31	0.00	27.59	27.59	0.00
16	0.09	8.33	8.33	0.00	0.75	0.75	0.00
Sum of absolute error				0.00			0.00
RMSE				0.00			0.00
Case 7: T_m = 75° C and G = 1000 W/m^2							
1	26.90	0.23	0.23	0.00	6.19	6.19	0.00
2	26.21	1.46	1.46	0.00	38.27	38.27	0.00
3	25.44	2.75	2.75	0.00	69.96	69.96	0.00
4	24.49	4.15	4.15	0.00	101.63	101.63	0.00
5	23.56	5.33	5.33	0.00	125.57	125.57	0.00
6	22.46	6.43	6.43	0.00	144.42	144.42	0.00
7	21.33	7.22	7.22	0.00	154.00	154.00	0.00
8	19.94	7.81	7.81	0.00	155.73	155.73	0.00
9	18.62	8.14	8.14	0.00	151.57	151.57	0.00
10	17.03	8.25	8.25	0.00	140.50	140.50	0.00
11	14.96	8.33	8.33	0.00	124.62	124.62	0.00
12	11.72	8.38	8.38	0.00	98.21	98.21	0.00
13	8.88	8.40	8.40	0.00	74.59	74.59	0.00
14	5.92	8.42	8.42	0.00	49.85	49.85	0.00
15	3.28	8.43	8.43	0.00	27.65	27.65	0.00
16	0.11	8.46	8.46	0.00	0.93	0.93	0.00
Sum of absolute error				0.00			0.00
RMSE				0.00			0.00

References

Abdel-Basset, M., Mohamed, R., Sharawi, M., et al. (2022). A comparative study of optimization algorithms for parameter estimation of pv solar cells and modules: Analysis and case studies. *Energy Reports, 8*, 13047–13065. https://doi.org/10.1016/j.egyr.2022.09.193

ABSOLAR (2024). Panorama da solar FV no Brasil e no mundo. https://www.absolar.org.br/mercado/infografico/, accessed on 03/04/2024.

Ahmed, E. M., Aly, M., Mostafa, M., et al. (2023). An accurate model for bifacial photovoltaic panels. *Sustainability, 15*(1) . https://doi.org/10.3390/su15010509

Batzelis, E., Blanes, J. M., Toledo, F. J., et al. (2022). Noise-scaled euclidean distance: A metric for maximum likelihood estimation of the pv model parameters. *IEEE Journal of Photovoltaics, 12*(3), 815–826. https://doi.org/10.1109/JPHOTOV.2022.3159390

Cari, E. P. T., Theodoro, E. A. R., Mijolaro, A. P., et al. (2009). Trajectory sensitivity method and master-slave synchronization to estimate parameters of nonlinear systems. *Mathematical Problems in Engineering, 2009*, 5532–5544. https://doi.org/10.1155/2009/387317

Diab, A. A. Z., Sultan, H. M., Aljendy, R., et al. (2020). Tree growth based optimization algorithm for parameter extraction of different models of photovoltaic cells and modules. *IEEE Access, 8*, 119668–119687. https://doi.org/10.1109/ACCESS.2020.3005236

El-Naggar, K., AlRashidi, M., AlHajri, M., et al. (2012). Simulated annealing algorithm for photovoltaic parameters identification. *Solar Energy, 86*(1), 266–274. https://doi.org/10.1016/j.solener.2011.09.032

Eslami, M., Akbari, E., Seyed Sadr, S. T., et al. (2022). A novel hybrid algorithm based on rat swarm optimization and pattern search for parameter extraction of solar photovoltaic models. *Energy Science & Engineering, 10*(8), 2689–2713. https://doi.org/10.1002/ese3.1160

Gameiro, M. F., & Rodrigues, H. M. (2001). Applications of robust synchronization to communication systems. *Applicable Analysis, 79*(1–2), 21–45. https://doi.org/10.1080/00036810108840950

Gao, S., Wang, K., Tao, S., et al. (2021). A state-of-the-art differential evolution algorithm for parameter estimation of solar photovoltaic models. *Energy Conversion and Management, 230*, Article 113784. https://doi.org/10.1016/j.enconman.2020.113784

Hara, S., Douzono, H., Imamura, M., et al. (2022). Estimation of photovoltaic cell parameters using measurement data of photovoltaic

module string currents and voltages. *IEEE Journal of Photovoltaics, 12*(2), 540–545. https://doi.org/10.1109/JPHOTOV.2021.3135262

Huang, Y. C., Huang, C. M., Chen, S. J., et al. (2020). Optimization of module parameters for pv power estimation using a hybrid algorithm. *IEEE Transactions on Sustainable Energy, 11*(4), 2210–2219. https://doi.org/10.1109/TSTE.2019.2952444

Huynh, D. C., Dunnigan, M. W., & Barbalata, C. (2022). Estimation for model parameters and maximum power points of photovoltaic modules using stochastic fractal search algorithms. *IEEE Access, 10*, 104408–104428. https://doi.org/10.1109/ACCESS.2022.3210687

Jiao, S., Chong, G., Huang, C., et al. (2020). Orthogonally adapted harris hawks optimization for parameter estimation of photovoltaic models. *Energy, 203*, Article 117804. https://doi.org/10.1016/j.energy.2020.117804

Kumar, C., & Magdalin Mary, D. (2022). A novel chaotic-driven tuna swarm optimizer with newton-raphson method for parameter identification of three-diode equivalent circuit model of solar photovoltaic cells/modules. *Optik, 264*, Article 169379. https://doi.org/10.1016/j.ijleo.2022.169379

Long, W., Cai, S., Jiao, J., et al. (2020). A new hybrid algorithm based on grey wolf optimizer and cuckoo search for parameter extraction of solar photovoltaic models. *Energy Conversion and Management, 203*, Article 112243. https://doi.org/10.1016/j.enconman.2019.112243

Lopes, S. M. A., Cari, E. P. T., & Hajimirza, S. (2021). A comparative analysis of ANN for photovoltaic power forecast using remotes and local measurements. *Journal of Solar Energy Engineering, 144*(2). https://doi.org/10.1115/1.4053031

Luo, W., & Yu, X. (2022). Quasi-reflection based multi-strategy cuckoo search for parameter estimation of photovoltaic solar modules. *Solar Energy, 243*, 264–278. https://doi.org/10.1016/j.solener.2022.08.004

Ma, J., Hong, D., Wang, K., et al. (2022). Analytical modeling and parameter estimation of photovoltaic strings under partial shading conditions. *Solar Energy Materials and Solar Cells, 235*, Article 111494. https://doi.org/10.1016/j.solmat.2021.111494

Nguyen, T. T., Nguyen, T. T., & Tran, T. N. (2022). Parameter estimation of photovoltaic cell and module models relied on metaheuristic algorithms including artificial ecosystem optimization. *Neural Computing & Applications, 34*(15, SI), 12819–12844. https://doi.org/10.1007/s00521-022-07142-3

Paul, K., Shekher, V., Kumar, N., et al. (2022). Influence of wind energy source on congestion management in power system transmission network: a novel modified whale optimization approach. *Process Integration and Optimization for Sustainability, 6*, 943–959. https://doi.org/10.1007/s41660-022-00271-1

Ramadan, A., Kamel, S., Hassan, M. H., et al. (2022). Accurate photovoltaic models based on an adaptive opposition artificial hummingbird algorithm. *Electronics, 11*(3). https://doi.org/10.3390/electronics11030318

Ramadan, H. A., Khan, B., & Diab, A. A. Z. (2022). Accurate parameters estimation of three diode model of photovoltaic modules using hunter-prey and wild horse optimizers. *IEEE Access, 10*, 87435–87453. https://doi.org/10.1109/ACCESS.2022.3199001

Ridha, H. M., Hizam, H., Mirjalili, S., et al. (2022). A novel theoretical and practical methodology for extracting the parameters of the single and double diode photovoltaic models. *IEEE Access, 10*, 11110–11137. https://doi.org/10.1109/ACCESS.2022.3142779

Rueda, J.L., & Erlich, I. (2013). Hybrid mean-variance mapping optimization for solving the IEEE- CEC 2013 competition problems. In 2013 IEEE Congress on Evolutionary Computation, https://doi.org/10.1109/CEC.2013.6557761.

Rueda, J.L., Gonzalez-Longatt, F., & Erlich, I. (2015). Online estimation of equivalent model for cluster of induction generators: A mvmo-based approach. In 2015 18th International Conference on Intelligent System Application to Power Systems, https://doi.org/10.1109/ISAP.2015.7325559.

Sager, B., & Erlich, I. (2017). Optimal allocation and sizing of capacitor banks for maximum power transfer to selected areas. In 2017 IEEE Manchester PowerTech, https://doi.org/10.1109/PTC.2017.7980965.

Sharadga, H., Hajimirza, S., & Cari, E. P. T. (2021). A fast and accurate single-diode model for photovoltaic design. *IEEE Journal of Emerging and Selected Topics in Power Electronics, 9*(3), 3030–3043. https://doi.org/10.1109/JESTPE.2020.3016635

Tchakpedeou, A.B., Lare, Y., & Napo, K., et al. (2022). An improved Levenberg–Marquardt Approach with a new reduced form for the identification of parameters of the one-diode photovoltaic model. Journal of Solar Energy Engineering 144(4). https://doi.org/10.1115/1.4053624.

Tong, N. T., & Pora, W. (2016). A parameter extraction technique exploiting intrinsic properties of solar cells. *Applied Energy, 176*, 104–115. https://doi.org/10.1016/j.apenergy.2016.05.064

Xiong, G., Li, L., Mohamed, A. W., et al. (2021). A new method for parameter extraction of solar pv models using gaining-sharing knowledge based algorithm. *Energy Reports, 7*, 3286–3301. https://doi.org/10.1016/j.egyr.2021.05.030

Xu, J. (2022). Separable nonlinear least squares search of parameter values in pv models. *IEEE Journal of Photovoltaics, 12*(1), 372–380. https://doi.org/10.1109/JPHOTOV.2021.3126105

Yu, S., Heidari, A. A., He, C., et al. (2022). Parameter estimation of static solar photovoltaic models using laplacian nelder-mead hunger games search. *Solar Energy, 242*, 79–104. https://doi.org/10.1016/j.solener.2022.06.046

Yu, S., Heidari, A. A., Liang, G., et al. (2022). Solar photovoltaic model parameter estimation based on orthogonally-adapted gradient-based optimization. *Optik, 252*, Article 168513. https://doi.org/10.1016/j.ijleo.2021.168513

Ćalasan, M., Abdel Aleem, S.H., & Zobaa, A.F. (2021). A new approach for parameters estimation of double and triple diode models of photovoltaic cells based on iterative lambert w function. *Solar Energy, 218*, 392–412. https://doi.org/10.1016/j.solener.2021.02.038.